Back to Session Subjects

IMPROVING HOVER PERFORMANCE OF LOW-TWIST ROTORS USING TRAILING-EDGE FLAPS - A COMPUTATIONAL STUDY

Adriano Gagliardi[1] and George N. Barakos[2]

[1]CFD Laboratory, Department of Aerospace Engineering
University of Glasgow, Glasgow G12 8QQ, United Kingdom
e-mail: a.gagliardi@aero.gla.ac.uk

[2]CFD Laboratory, Department of Engineering
University of Liverpool, Liverpool L69 3GH, United Kingdom
e-mail: G.Barakos@liverpool.ac.uk

Keywords: Flapped rotor, hover performance enhancement, HIMARCS I, ERF32

Abstract. This study evaluates the potential benefits that a slotted, trailing-edge flap may have for low-twist hovering rotors by combining a blade-element method with 2D and 3D Computational Fluid Dynamics (CFD). Low blade twist is beneficial in terms of forward flight performance, while a deployable flap could enhance hover performance resulting in an overall improved design in comparison to a standard rotor blade. A parametric study of numerous flap configurations was conducted and the resulting flapped rotors were compared against clean blades with various twist angles using a simple blade element method with CFD-generated sectional aerodynamics. This simple model indicated that up to 6^o of blade twist could be recovered at high thrust settings by using a slotted flap of dimensions 32% chord, 24% spanwise length, located at 48% blade span, and deflected by 10^o. Performance improvements were also obtained for outboard slotted flap configurations. The suggested optimum inboard and outboard flap configurations were subsequently evaluated in hover using 3D CFD. The obtained results confirmed the effectiveness of the inboard slotted flap combined with a low-twist (-7^o) rotor blade. This configuration matched the performance of an identical blade geometry with -13^o of twist.

Nomenclature

c	Non-dimensional blade chord
C_T	Thrust coefficient, $C_T = \frac{T}{\rho\pi R^2(\Omega R)^2}$
C_Q	Torque coefficient, $C_Q = \frac{Q}{\rho\pi R^3(\Omega R)^2}$
FM	Figure of merit, $FM = 0.707\frac{C_T^{1.5}}{C_Q}$
P	Non-dimensional pressure , $P = \frac{p^*}{\rho^*_\infty U^{*2}_\infty}$
a_{ij}	Acceleration tensor
Ω	Vorticity tensor
BVI	Blade-Vortex Interaction
CAD	Computer-Aided Design
CFD	Computational Fluid Dynamics
CPU	Central Processing Unit
FEV	Flap-edge vortex
R	Non-dimensional blade span, $R = \frac{R^*}{c^*}$
β_0	Coning angle [deg]
δ	Flap deflection angle [deg]
θ_0	Collective pitch at 0.75R [deg]
ρ	Density [kg/m^3]
Re	Reynolds number, $Re = \frac{\rho U c}{\mu}$
S	Strain rate tensor
HIMARCS	High 0 and Agility Rotor and Control System
HMB	Helicopter Multi-Block
URANS	Unsteady Reynolds-Averaged Navier-Stokes

1 INTRODUCTION

The design of rotors is a complex task where hover and forward-flight performances must be balanced. For example, good hover performance can be obtained using high levels of blade twist, but this may induce further penalties in fast forward flight. On the advancing side of the rotor disc, low blade tip angles can lead to losses in propulsive force and exacerbate compressibility effects [1]. To help eliminate these design restrictions, new technologies such as Active Flap Control (AFC) are currently under development. Such technologies could allow future rotorcraft to offer reduced vibrations, reduced Blade-Vortex Interaction (BVI) noise, and increased lifting capabilities. Proving successful, a new generation of helicopters would be able to offer near jet-smooth rides, improved environmental acceptance, and greater mission scope.

In this work, the use of fixed flaps in hover is considered and analysed. So far, deployment of a fixed flap in hover has received little exposure in the literature as opposed to actuated flaps for vibration reduction. The technology demonstration of the Controllable Twist Rotor (CTR) implemented on Kaman aircraft carried out by Lemnios and Howes [2] at the NASA Ames Research Centre mainly offered improved rotor performance in forward flight, although whirl-tower tests were conducted in hover. Negative flap deflections (flap up) of -4^o and -8^o were used with a linear decrease in hover performance exhibited. No results for positive flap deflections were published. More recently, Ormiston and Fulton [3] investigated the aeroelastic phenomenon of elevon reversal that can occur when flaps are used on twist control blades with low-torsional stiffness. Unfortunately, although testing was carried out in hover, no performance data was presented. Rotor aeroelastic investigations were also conducted by Koratkar and Chopra [4] who tested a piezo-ceramic actuation device for application to vibration reduction, but no aerodynamic performance data was presented either. However, in 2001 Noonan *et al.* [5] looked at fixed flow-control devices located at the blade tip for performance enhancement and blade-loads reduction in hover and forward flight using the High 0 and Agility Rotor and Control System (HIMARCS I) rotor blade (see Figure 1). Their work focused on reducing the required levels of blade twist and recuperating the loss in hover performance by deflecting (or extending) a trailing-edge flap downwards (positive deflection). When transferring to forward flight, the flap may then be returned to its neutral position and improved forward flight performance can be obtained with reduced compressibility effects and greater thrust at the advancing blade tip. They considered a low-twist blade (-7^o of linear twist) with a 3^o slotted flap located in the tip region, as well as two leading-edge slat configurations. Good reductions in the 4/rev pitch-link loads were recorded using the 3^o slotted flap, although it was ineffective in improving the thrust-to-torque ratio. Wachspress and Quackenbush [6] considered fixed, inboard flaps for reducing BVI noise in low-speed descent using the CHARM analysis tool. They demonstrated that noise reduction was possible at certain flight conditions due to various mechanisms that weakened the vortex core strength and altered the vortex trajectory. Wind-tunnel tests appeared to support their results. The most recent research into the use of flapped rotors in hover was published by the authors [7] and, to our knowledge, it is the only computational work in the open literature where a fixed flap has been considered for hover performance improvements.

The current research follows on from Ref. [7] and is concerned with a computational study of flapped rotor blades in hover. Blade element and CFD methods were used in combination as shown in Figure 2. The whole process began by generating the necessary aerodynamic data for the rotor blade sections via 2D CFD and relying on the blade element method for calculating the performance data and trim settings of the full rotor. The results were evaluated and, after deciding on the optimum flap configuration, specific cases were selected and computed using 3D CFD.

2 MATHEMATICAL MODELLING

The analysis of flapped rotors in hover requires the rapid computation of many flap configurations and comparisons with clean blades for a range of thrust settings. Given the CPU demands of CFD it would be more efficient if a faster method was used to obtain an approximate optimum flap configuration before detailed CFD computations are undertaken. A blade element method is suitable for rapid hover calculations provided adequate aerodynamic data for the clean and flapped blade sections are available. Without adequate wind tunnel data, 2D Unsteady Reynolds-Averaged Navier-Stokes (URANS) CFD computations were used to generate all the aerodynamic input required by the blade element method. The current work utilised the original HIMARCS I rotor geometry [5] as well as CAD-modified geometries to take into account variable flap chord lengths and deflection angles. A brief description of the blade element and CFD methods employed in this work is given in the following paragraphs.

2.1 Blade element method

The blade-element method calculates the local loading at a series of radial stations on a rotor blade for a given azimuth, followed by integration and progressive stepping through the azimuth range. This method must be combined with a prescribed wake method to account for downwash. The rotor blade is first discretised into sections, with each requiring geometric and aerodynamic data to be supplied as input. For this work, aerodynamic data at Mach numbers ranging from 0.3 to 0.9 were used and these included stall angles, zero-lift angles, lift-curve slopes, as well as information for the pre- and post-stall moment behaviour. The required geometric data included information for the radial variation of the chord lengths, blade twist, and sweep angles. A prescribed wake was used with a fixed contraction ratio. The method has been detailed in Ref. [8] for clean blades and was applied here for flapped rotors.

2.2 Computational fluid dynamics

All CFD computations were performed using the Helicopter Multi-Block (HMB) flow solver [9] developed at the University of Glasgow. The solver has been successfully applied to a variety of problems including rotorcraft in hover and forward flight [10], dynamic stall [11], and BVI [12]. HMB solves the 2D and 3D URANS equations on multi-block structured grids in serial or parallel mode. The governing equations are discretised using a cell-centred finite volume method. The convective terms are discretised using either Osher's or Roe's scheme. MUSCL interpolation is used to provide formally third order accuracy and the Van Albada limiter is used to avoid spurious oscillations across shocks. The time-marching of the solution is based on an implicit, dual time stepping method. The final algebraic system of equations is solved using a Conjugate Gradient method, in conjunction with Block Incomplete Lower Upper factorisation. A number of one and two equation turbulence models are available, as well as Large Eddy Simulation and Detached Eddy Simulation. The viscous computations in the current work were performed using the Wilcox k-ω turbulence model [13].

To improve the quality of the flowfield visualisations, the parameter λ_2 was used to clearly capture the vortical structures in the near wake of the rotors [14]. It locates pressure minima due only to vortical motion and is derived from taking the gradient of the incompressible Navier-Stokes equations. Expressing this in terms of the pressure Hessian we have:

$$-\frac{1}{\rho}p_{,ij} = a_{ij} + \nu u_{i,jkk} \tag{1}$$

From term a_{ij}, the acceleration tensor, the antisymmetric part which describes inviscid vorticity transport is assumed to be satisfied and the second term of Equation 1 is ignored, including any unsteady terms. Equation 1 then simplifies to:

$$-\frac{1}{\rho}p_{,ij} = \Omega^2 + \mathbf{S^2} \tag{2}$$

Taking the second derivative of Equation 2 to find the local maxima or minima, the low pressure found in vortex cores could be obtained when the second largest eigenvalue, λ_2, is less than zero.

3 RESULTS AND DISCUSSION

3.1 Summary of assessed designs

Table 1 presents a comparison between the necessary CPU time for the analysis based on the blade element and CFD methods. As expected, the CPU time for the blade element computations is a fraction of that required by CFD. Consequently, the blade element method was used to perform calculations for a range of flap configurations. The flap parameters selected for investigation were: (a) flap deflection angle, (b) flap location, (c) flap chord-wise length, and (d) flap span-wise length. Slotted flap configurations geometrically-equivalent to the designs employed in the HIMARCS I paper were considered in this work. Flap chord sizing was accomplished via direct scaling of the original flap geometry, which was then super-positioned on both clean sections with the approximate slot geometry accounted for in the same way. Table 2 presents the variations applied to each parameter and the overall number of assessed designs, with the blade span, R, taken from the shaft axis to the blade tip, as defined in Figure 1. Although the blade element method is efficient, it depends on aerodynamic inputs, unlike CFD. For this reason, every flap configuration had to be tested in 2D using CFD and a database was collected to serve as a lookup table for the blade element method. It has to be noted that the 2D nature of the CFD computations employed for extracting the aerodynamic parameters for the blade element method allowed for computations to be performed on low-power workstations and required no parallel computing.

3.2 Grid generation - 2D and 3D configurations

The employed CFD method requires multi-block structured grids of high quality with all grids in the current work generated using the ICEMCFD-*Hexa* package. Several topologies had to be considered and these are summarised in Table 3 (2D grids) and Table 4 (3D grids). The HIMARCS I rotor is made out of two sections, the RC(4)-10 [16] from 22.4%R to 80%R, transition from 80%R to 85%R, and the RC(6)-08 [15] from 85%R-100%R, with -7^o of unoptimised twist from the root cut-out to the blade tip. Both had to be considered with and without flaps. For a clear section C-type grids are adequate for CFD analysis. Flapped sections, however, require more general multi-block topologies like the C-C one employed in this work. Figure 3 presents typical 2D grid configurations. Care had been taken to allow the constructed grids to be deformed to account for the deflection of the flap so that the minimum number of CFD grids were constructed. The details of the 2D grids in terms of number of points, configurations and distribution of points are shown in Table 3. The same care was necessary for the generation of 3D grids. The far-field boundary is equivalent to a quarter-cylinder with the rotor in the centre, as shown in Figure 4. The employed grids have a C-type topology near the blade which evolves to H-type away from the body (see Figure 5(a)). Single-bladed grids were generated with periodic boundaries to account for the 4-bladed configurations considered. The blade was treated as rectangular and the topology employed at the tip was similar to the one used in Ref. [11]. The root cut-out section was not modelled. The advantage of this configuration is that it allows flat and rounded tips, and it can be modified to account for the presence of integrated and slotted flaps. The surface mesh and block boundaries near the inboard and outboard flaps are shown in Figure 5(c)-(f). For the slotted case, blocks are placed between the main section and the flap and a small gap of 1%R was used to allow for the flap to be deflected. The inviscid and viscous grids were constructed with wall distances as described in Table 4.

3.3 Parametric study of the flap configurations

Figure 6(a) presents typical CFD results for the lift, drag and moment coefficients obtained from quasi-steady ramping calculations. Such plots allowed the extraction of the stall angles, lift-slope and post-stall behaviour of all tested configurations. The results were computed using the Wilcox k-ω model with free transition. Grid convergence for the drag coefficient was obtained. Such results are only approximate since transition is not accounted for and the k-ω model may under-predict stall. However, only relative differences are considered in this work between the various designs. The flowfield for the 32%c slotted flap configuration can be seen in Figure 6(b), where isomachs are used to highlight the presence of the boundary layer and shocks in the slot cavity.

Typical results from the parametric study with the blade element method are shown in Figure 7, with the full compliment of the design range considered listed in Table 2. Due to the number of parameters involved, a 5-dimensional plot would be necessary. Instead, the results are first compared at two flap deflection angles (3^o and 10^o) with varying flap location and span for the standard flap chord of 32%c. A flap angle of 6 degrees was also considered though results varied in an almost linear fashion. The target C_T = 0.00713 and the baseline Figure of Merit (FM) was 0.7623. As can be seen from the contours of FM in Figure 7(c), the inboard flap has an optimum location near 48% of the rotor radius while the span of the flap should not exceed 24%R with a flap deflection angle, $\delta = 10^o$. This process was repeated for flap chords of 21.33%c and 11.67%c, over a range of 15 C_T's. The effect of decreasing flap chord resulted in a linear decrease in hover performance with a very small improvement at very low C_T's. In most cases, there were 3 or 4 designs that could have been implemented. Therefore, a decision was made to select a flap design that was located sufficiently inboard i.e. avoided the blade root and allowed for a closed blade tip, unlike the original HIMARCS flapped rotor. The flaps selected were: (a) inboard, flap location: 48%c, flap span: 24%R, flap chord: 32%c, and flap deflection angle: 10^o, and (b) outboard, flap location: 94%R, flap span: 6%R, flap chord: 32%R, flap deflection angle: 10^o.

A summary of the findings of the parametric study is presented in Figure 8, where the computed FM using the blade element method for the flapped configurations is compared against the clean HIMARCS I blade with -7^o and -13^o of twist. The schematic of the same figure shows the selected best-fit inboard and outboard flap configurations. It is evident that the flapped rotor did not help at low thrust settings. Results for mid to high thrust settings were, however, very encouraging indicating increases of 3-10% in hover performance.

3.4 3D hover CFD - validation

For this work, results have been obtained for the hovering HIMARCS I rotor without the Aeroelastic Rotor Experimental System (ARES) fuselage, using inviscid and viscous CFD. The employed grids are detailed in Table 4. Computations were performed on a Beowulf cluster consisting of 120 2.4-3Ghz Pentium 4 nodes with 1GB RAM each. For most cases, 8-25 processors were used. Viscous computations were, as expected, more demanding in terms of CPU time, but provided results closer to the NASA data [5]. The details of the CPU time required for all computations can be found in Table 1. For accuracy, all 3D computations were run until the FM prediction was roughly constant with around 8000-14000 time steps necessary to achieve this (less time steps were required at higher blade loadings).

Figure 9(a)-(b) presents the comparison between CFD and experimental data for the rotor's C_T, C_Q, and FM. In addition, the collective and coning angles predicted by the blade element method and used for the CFD simulations are shown in Figure 9(c). As can be seen, the viscous results provided better thrust and torque estimates at medium-high blade loadings, which were over-estimated by the inviscid solutions. However, the inviscid results were adequate for comparisons between similar designs up to low-moderate thrust settings and, in addition, inviscid computations were found to be more economic in terms of CPU time. It must also be considered that for the experiment a generic helicopter fuselage was also present. For simplicity, the fuselage was not included in this work and, therefore, the obtained results were expected to deviate from the experimental data, especially for the higher thrust settings.

3.5 3D hover CFD - effect of blade twist

To quantitatively assess the effect of twist on the obtained hover results, two CFD grids were put together for blades with linear twists of -4^o and -13^o, respectively. Inviscid computations for a range of thrust settings between 0.002 and 0.0082 were undertaken, and the obtained results were compared against the datum HIMARCS I blade with -7^o of twist. The inviscid results for the C_T, C_Q, and FM are presented in Figure 10(a)-(b). As can be seen, the highly twisted blade has an advantage at moderate to high thrust settings with the differences between the -7^o and -13^o blades diminishing at low thrust values. The blade with -4^o of twist is shown to be less efficient compared to the more highly twisted blades. To further establish this conclusion, viscous computations were performed for the blades with -7^o and -13^o of twist (see Figure 10(c)-(d)). These results established confidence in the CFD method and helped quantify the effect of blade twist in hover in terms of FM. In addition, the obtained results set a standard for expected performance from the flapped rotor. Ideally, the flapped blade with just -7^o of twist should meet or exceed the performance of the highly twisted (-13^o) rotor.

3.6 3D hover CFD - flapped rotors

The optimum flap configurations suggested by the blade element theory were implemented on CFD grids for the inboard and outboard configurations. The details of the grids are shown in Table 4. Every effort was made not to add a substantial amount of points on the flapped rotors, so that the comparison against the clean designs was as fair as possible. However, due to the complexity of the employed multi-block topology, the requirements to model the near flap region, as well as to resolve the flap loading, an increase in the number of points was necessary. CFD results, including the trim states, were obtained for the 3^o slotted flap case and the optimum blade designs for a whole range of thrust settings. These are plotted in Figure 11(a)-(c) along with the results for the clean rotors with -7^o and -13^o of twist. The optimum inboard flap is shown to match and exceed the performance of the highly twisted blade for high thrust settings, which confirms the predictions of the blade element method. Another encouraging result is that the optimum inboard flap design equalled the performance of the -13^o twisted blade, but with reduced collective and coning angles (between 0.5^o-1^o). An inboard flap shows promise, especially as it would not have an effect on the design of the blade tip shape. The outboard flap configuration, however, under-performs compared to blade element predictions, but still improves on the outboard flap design tested at NASA [5]. This includes similar savings in blade trim angles as the inboard flap (see Figure 11(c)). Further examination of the results identified the poor performance of the outboard slotted flap as being due to the increased strength of the trailed Flap-Edge Vortices (FEV) the further outboard the flap is located. The induced losses at the flap edges combined with the small flap size led to the CFD underpredicting the blade element method, which does not take induced power losses due to the flap downwash into account. It must also be noted that the size of the flap gap in the CFD was not optimised and may have hindered performance.

Figure 12 plots iso-surfaces of λ_2 to visualise the CFD-predicted vortices in the near wake of the baseline HIMARCS I rotor, the HIMARCS I with 3^o slotted flap, and the two optimised flapped configurations. Interestingly, we can see the amalgamation into a larger structure, which passes below the blade, of the two co-rotating vortices trailed from the blade tip and the flap-edge of the two outboard flap designs. The trailed vortices inboard also pass under the blade, but notably more distant than those outboard. This may result in higher induced loadings on the fuselage due to interactions with the inboard vortices. Further analysis of the rotor downwash is required for this issue to be clarified.

3.7 3D hover CFD - effect of flap

Figure 13 presents the non-dimensional pressure distribution over the area of the baseline blade and the inboard flap optimised blade. It is clear from the plots that there is generally good agreement between the flapped (Figure 13(b)) and baseline grids (Figure 13(a)) in regions away from the flap. Most of the flap contribution is also evident, although its effect on the main-element is harder to quantify. Further analysis indicated that the suction peak on the flap happens to occur directly below the trailing-edge of the main-element (see Figure 14). This downforce on the lower surface of the main element's trailing-edge gives a reduction in lift, although the net increase due to the flap is still positive. Moving the expected suction peak location away from the main element's trailing-edge is expected to result in greater increases in lift albeit with increased nose-down pitching moments.

4. SUMMARY AND FUTURE WORK

Blade element and CFD methods have been employed for the assessment of a new flapped rotor concept. A fixed flap was deployed on a low twist rotor blade and its location, chord, spanwise length, and deflection angle were evaluated, resulting in a new configuration. The final design was comparable in hover performance with a clean rotor blade with -13^o of twist.

The inboard flap configuration was found to be beneficial at high thrust settings by the blade-element method, a result that was confirmed by the 3D CFD. The outboard flap configuration was shown to be less effective, possibly due to the lack of modelling of certain flow physics in the blade-element method that are important outboard where the air velocity and torque arm are greater. The results are encouraging and suggest that a fixed flap deployed in hover may offer a good balance between forward flight and hover performances for future designs. Further work is, however, necessary to better understand the overall effects of the flap in the rotor flow environment. Future research should consider the downwash distribution below the rotor and attempt to quantify the effect of the flap on the fuselage loadings, as well as the effect of the flap location on the pitch-link loads.

Acknowledgements

This research is sponsored by Westland Helicopters Limited and the University of Glasgow.

References

[1] C. Keys, F. Tarzanin, and F. McHugh, ”Effect of Twist on Helicopter Performance and Vibratory Loads”, 13th European Rotorcraft Forum, Arles, France, September 1987.

[2] A.Z. Lemnios, and H.E. Howes, ”Wind Tunnel Investigation of the Controllable Twist Rotor Performance and Dynamic Behaviour”, USAAMRDL-TR-77-10, June 1997.

[3] R.A. Ormiston, and M.V. Fulton, ”Aeroelastic and Dynamic Rotor Response with On-Blade Elevon Control”, 24th European Rotorcraft Forum, Marseilles, France, September 1998.

[4] N.A. Koratkar, and I. Chopra, ”Wind Tunnel Testing of a Smart Rotor Model with Trailing-Edge Flaps”, Journal of the American Helicopter Society, Vol. 47(4), October 2002, pp. 263-272.

[5] K.W. Noonan, W.T. Yeagar, J.D. Singleton, M.L. Wilbur, and P.H. Mirick, ”Wind Tunnel Evaluation of a Helicopter Main-Rotor Blade with Slotted Airfoils at the Tips”, NASA-TP-2001-211260, December 2001.

[6] D.A. Wachspress, and T.R. Quackenbush, ”BVI Noise Mitigation Via Steady Flap Deflection - An Analysis-Led Test Program”, American Helicopter Society 4th Decennial Specialist’s Conference on Aeromechanics, San Francisco, USA, January 2004.

[7] A. Gagliardi, J. Beedy, R. Steijl, G.N. Barakos, and K.J. Badcock, ”Analysis of Flapped Rotors Using CFD and Indicial Methods”, American Helicopter Society 61st Annual Forum, Grapevine, Texas, USA, June 2005.

[8] J. Beedy, G.N. Barakos, K.J. Badcock, and B.E. Richards, ”Using CFD to Improve the WHL Rotor Load Aerodynamic Model”, 30th European Rotorcraft Forum, Marseilles, France, September 2004.

[9] K.J. Badcock, B.E. Richards, and M.A. Woodgate, ”Elements of Computational Fluid Dynamics on Block Structured Grids Using Implicit Solvers”, Progress in Aerospace Sciences, Vol. 36(5-6), July-August 2000, pp. 351-392.

[10] R. Steijl, G.N. Barakos, and K.J. Badcock, ”A Framework for CFD Analysis of Rotors in Hover and Forward Flight”, International Journal for Numerical Methods in Fluids, 2006. (in press)

[11] A. Spentzos, G.N. Barakos, K.J. Badcock, B.E. Richards, P. Wernert, S. Schreck, and M. Raffel, ”Investigation of Three-Dimensional Dynamic Stall Using Computational Fluid Dynamics”, AIAA Journal, Vol. 43(5), May 2005, pp. 1023-1033.

[12] R. Morvant, K.J. Badcock, G.N. Barakos, and B.E. Richards, ”Airfoil-Vortex Interaction Using the Compressible Vorticity Confinement Method”, AIAA Journal, Vol. 43(1), January 2005, pp. 63-75.

[13] D.C. Wilcox, ”Reassessment of the Scale-Determining Equation for Advanced Turbulence Models”, AIAA Journal, Vol. 26(11), November 1988, pp. 1299-1310.

[14] M. Roth, ”Automatic Extraction of Vortex Core Lines and Other Line-Type Features for Scientific Visualization”, Ph.D. thesis, ETH No. 13673, Institute of Scientific Computing, Computer Graphics Group, July 2000.

[15] K.W. Noonan, ”Aerodynamic Characteristics of a Rotorcraft Airfoil Designed for the Tip Region of a Main Rotor Blade”, NASA TM 4264, May 1991.

[16] K.W. Noonan, ”Aerodynamic Characteristics of Two Rotorcraft Airfoils Designed for Application to the Inboard Region of a Main Rotor Blade”, NASA TP 3009, July 1990.

Method	Grid Points	Processors*	Design Conditions	Time (in hours)
Blade-Element Method	-	1	≈7700	≈2.5
2D URANS CFD	85,000	1	40	≈6
3D Inviscid CFD	2.2M	8	1	≈20
3D Viscous CFD	2.7M	8	1	≈36

* 2.4-3Ghz P4 with 1GB DDR RAM.

Table 1: Grid size and CPU requirements for various methods.

	Flap Location	Flap Span	Flap Chord	Flap Deflection	Number of Designs
Inboard	28%R-68%R	4%R-24%R	32%c, 21.33%c, 10.67%c	3^o, 10^o	396 at 15 C_T's
Outboard	90%R-96%R	2%R-10%R	32%c, 21.33%c, 10.67%c	3^o, 10^o	120 at 15 C_T's

Table 2: Summary of the parameter space investigated.

Geometry	2D/3D	Grid Topology	Grid Blocks	Size	Points on Surface	Points on Flap	First Cell Distance
RC(6)-08	2D	C grid	6	83,000	360	-	10^{-5}c
RC(4)-10	2D	C grid	6	83,000	360	-	10^{-5}c
3^o Slotted Flap	2D	C-C grid	14	81,200	320	220	10^{-5}c
10^o Slotted Flap	2D	C-C grid	14	81,200	320	220	10^{-5}c

Table 3: 2D multi-block grid details used for viscous CFD calculations.

Geometry	Blocks	1st Cell Distance (Inv.) Main:Tips	Grid Points (Inv.) Blade:Flap:Total	1st Cell Distance (k-ω) Main:Tips	Grid Points (k-ω) Blade:Flap:Total
Clean Blade	106	10^{-4}c : 10^{-4}c	16k : 0 : 2.2M	10^{-5}c : 10^{-4}c	18k : 0 : 2.7M
3^o Slotted Flap	359	10^{-3}c : 10^{-3}c	20k : 1.3k : 2.6M	- : -	- : - : -
Optimised Flaps	446	10^{-3}c : 10^{-3}c	22k : 1.5k : 2.6M	- : -	- : - : -

Table 4: Details for 3D inviscid and viscous grids.

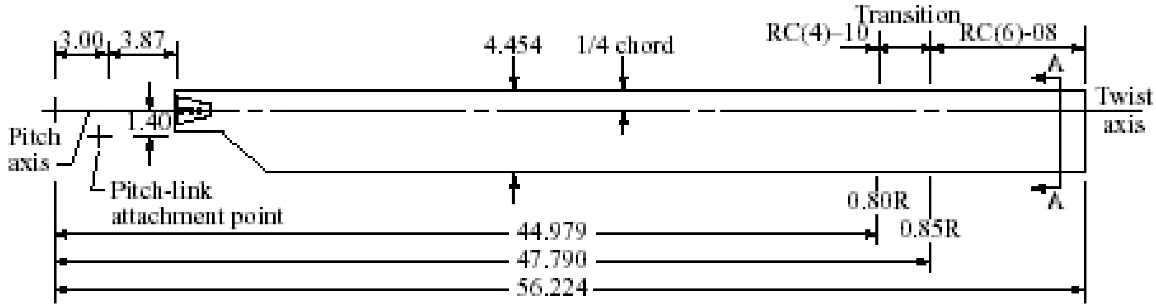

Figure 1: The HIMARCS I rotor blade geometry [5]. The blade span, R, is taken from the shaft to the blade tip. All values are in inches.

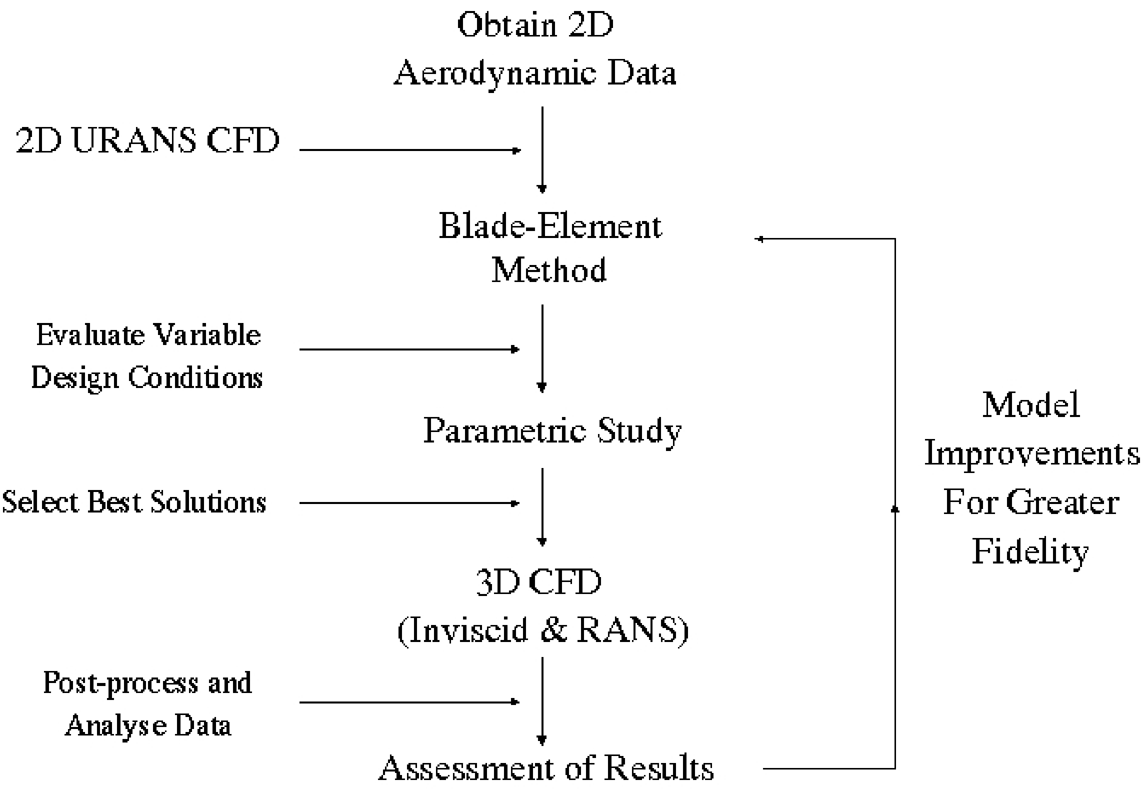

Figure 2: Employed methods for hover analysis of flapped rotors.

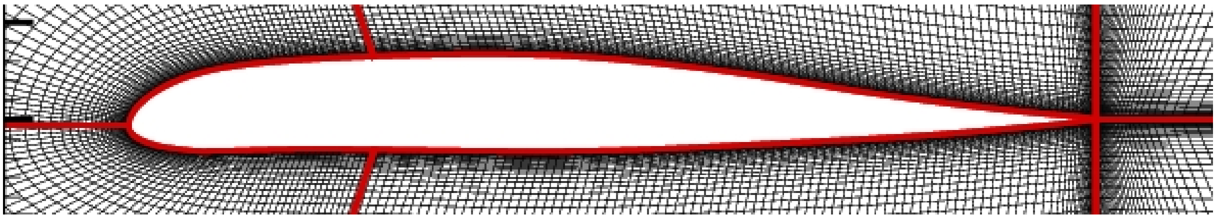

(a)

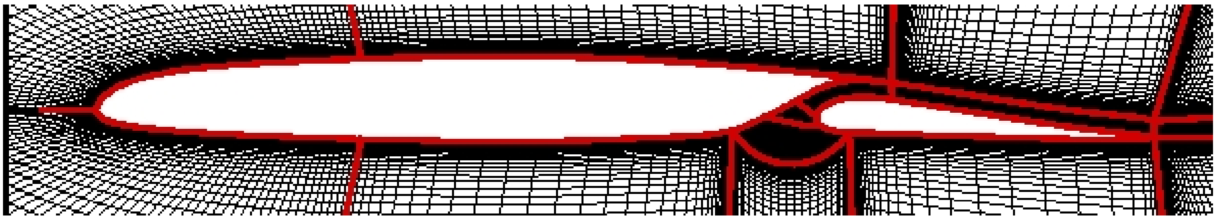

(b)

Figure 3: 2D multi-block grids. (a) RC(4)-10. (b) RC(6)-08 with 3^o slotted flap.

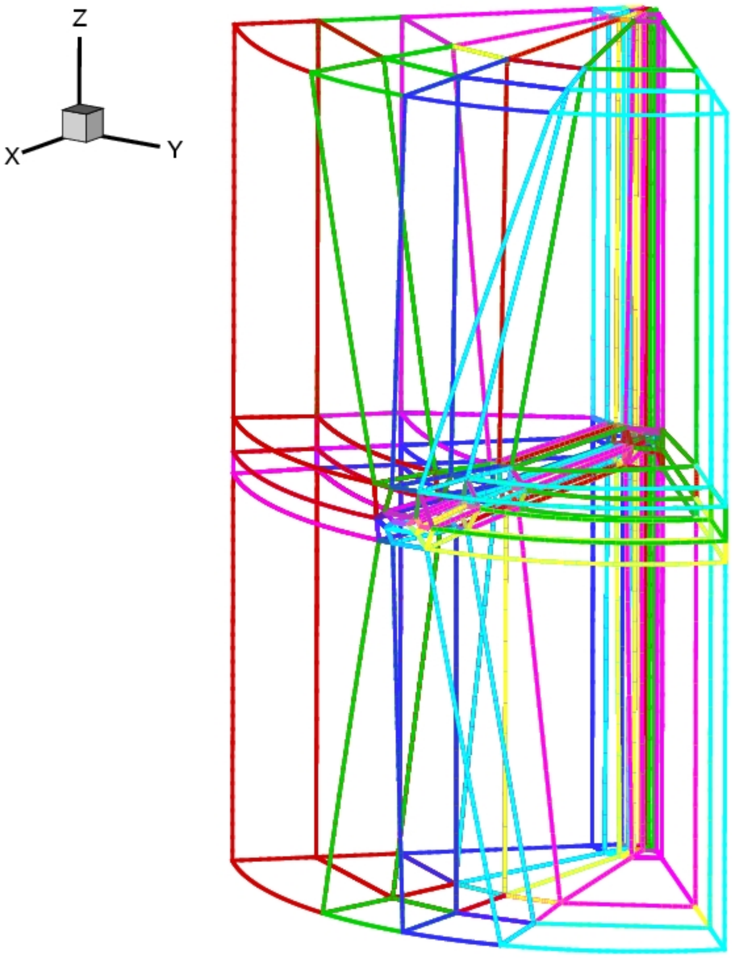

Figure 4: Example of 3D hover grid topology for a single-blade. All four blades are accounted for via periodic boundaries.

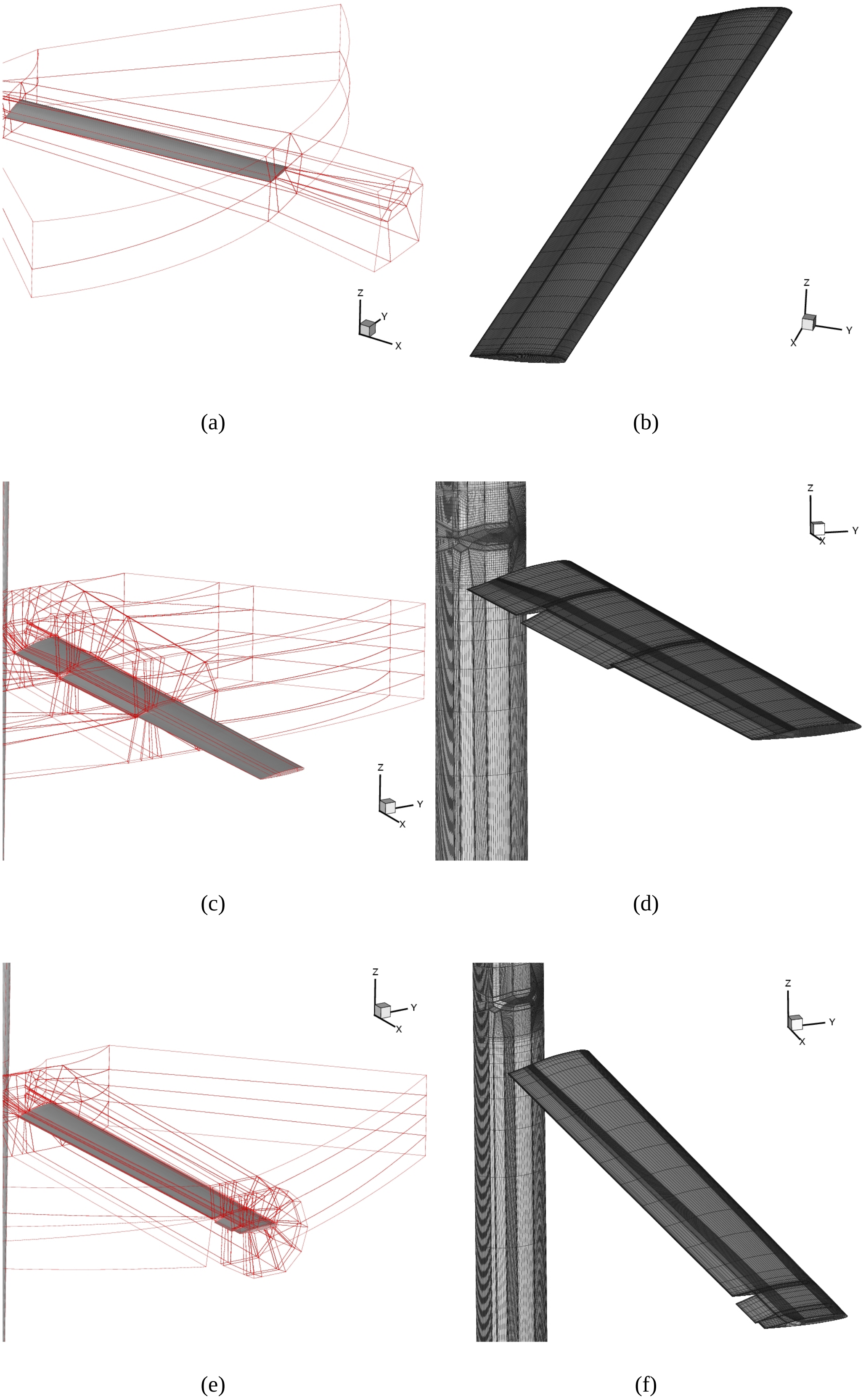

Figure 5: 3D multi-block topologies. Baseline: (a) C-H blocking. (b) Surface mesh. Inboard flap: (c) C-C-H blocking. (d) Surface mesh. Outboard flap: (e) C-C-H blocking. (d) Surface mesh.

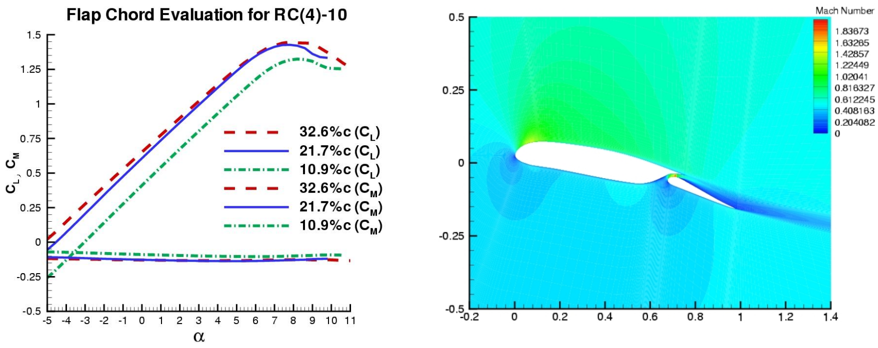

(a) (b)

Figure 6: 2D CFD results for optimisation study of the RC(4)-10 with 32%c slotted flap at α = 5^o and δ = 10^o. (a) C_L-α and C_M-α curves. (b) Mach contours. (M = 0.5, Re = 5x10^6)

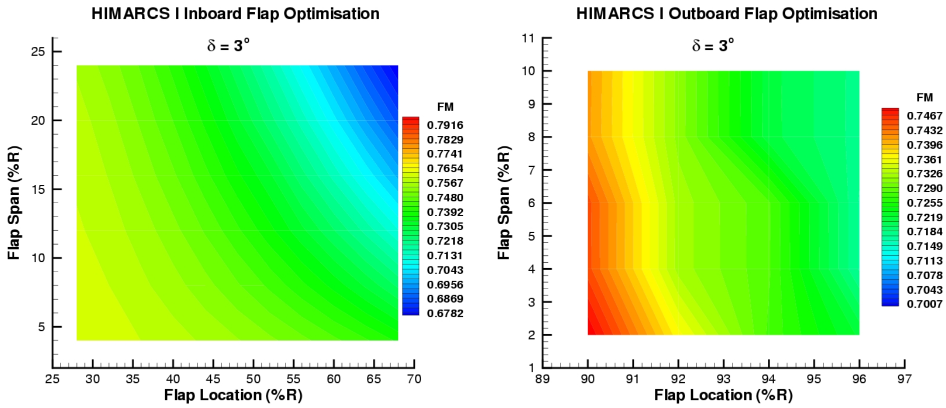

(a) (b)

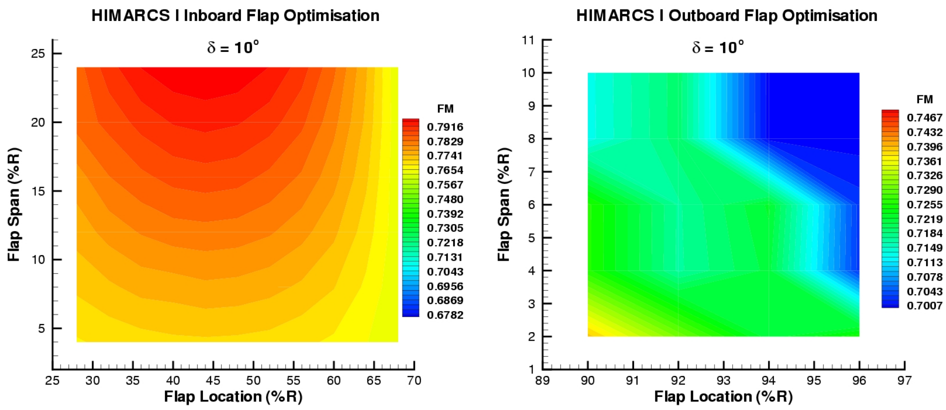

(c) (d)

Figure 7: HIMARCS I with trailing-edge flap optimised for Figure of Merit at C_T = 0.00713 (Baseline FM = 0.7623). (a) Inboard, δ = 3^o. (b) Outboard, δ = 3^o. (c) Inboard, δ = 10^o. (d) Outboard, δ = 10^o.

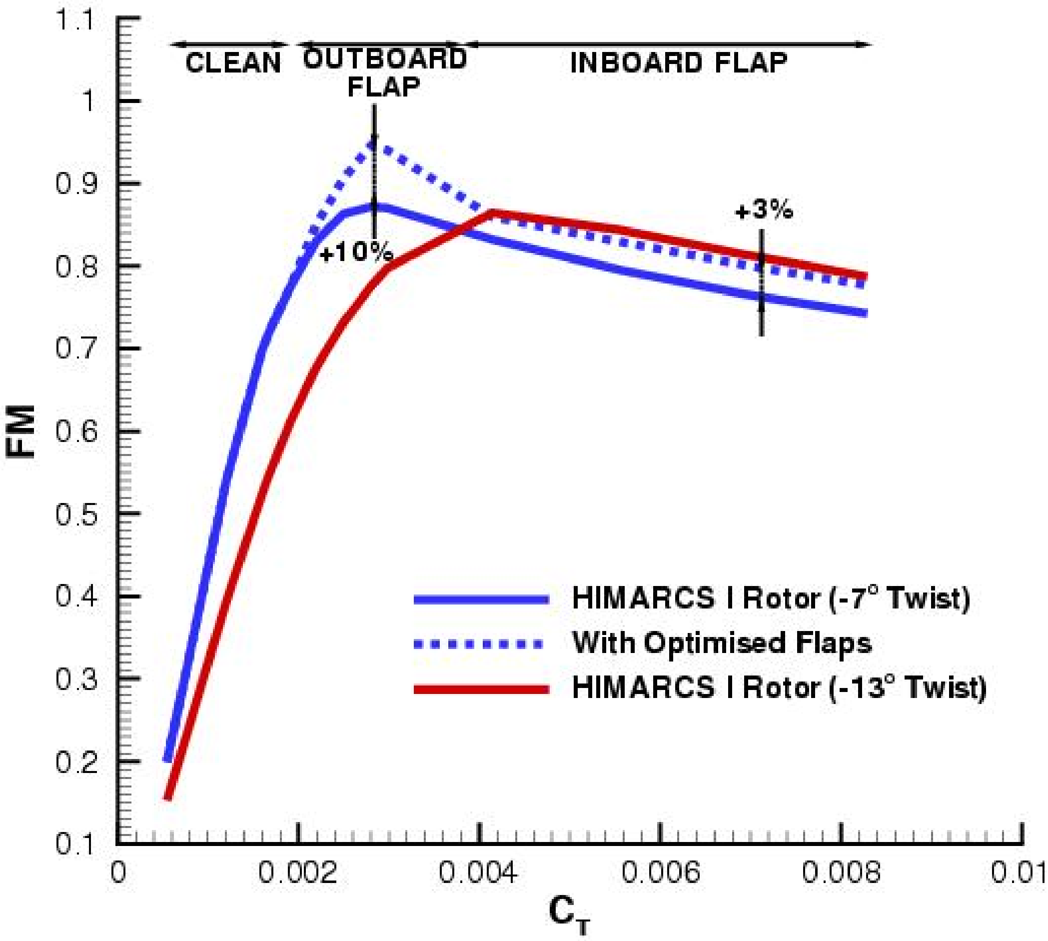

(a)

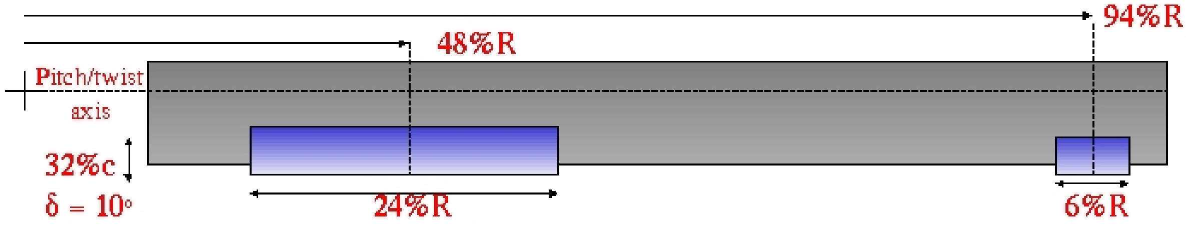

(b)

Figure 8: Optimum flap design. (a) Deployment schedule for fixed flaps in hover. (b) Schematic of HIMARCS I with optimised flaps.

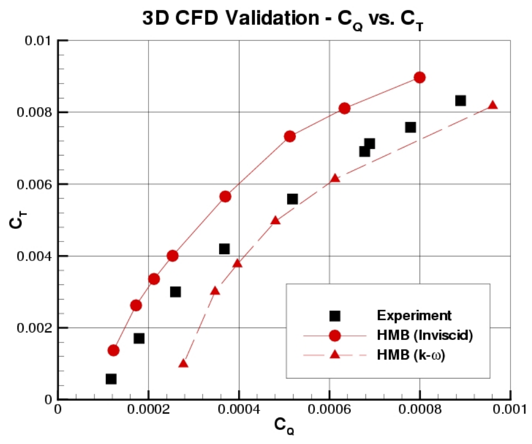

(a)

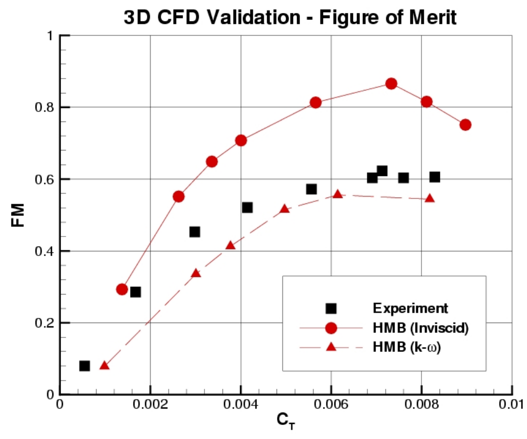

(b)

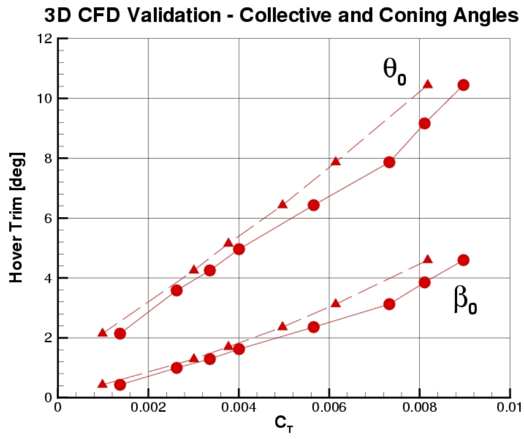

(c)

Figure 9: 3D CFD validation of the baseline HIMARCS I rotor. (a) C_Q vs. C_T. (b) C_T vs. FM. (c) C_T vs. Trim. (M_T = 0.627, Re = 168,602; blade collective taken at 0.75R.)

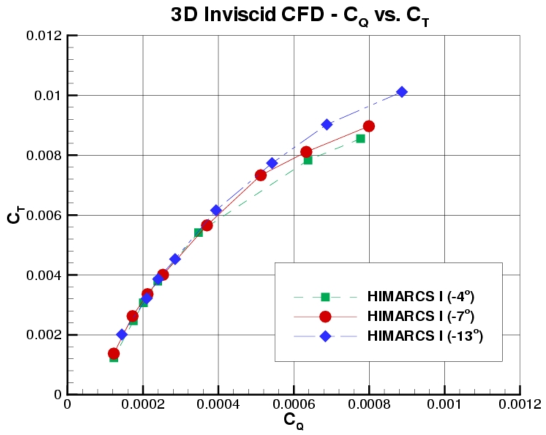

(a)

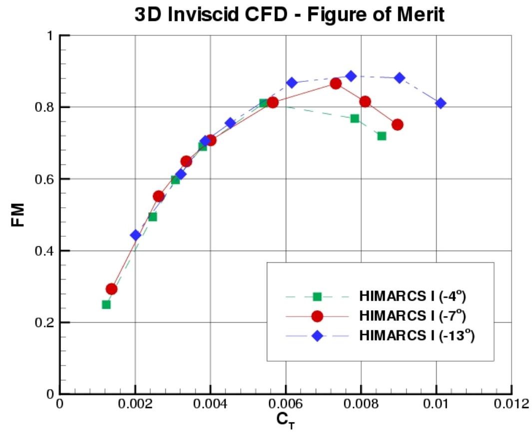

(b)

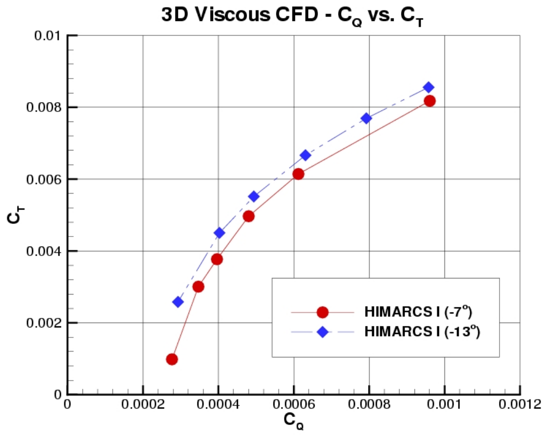

(c)

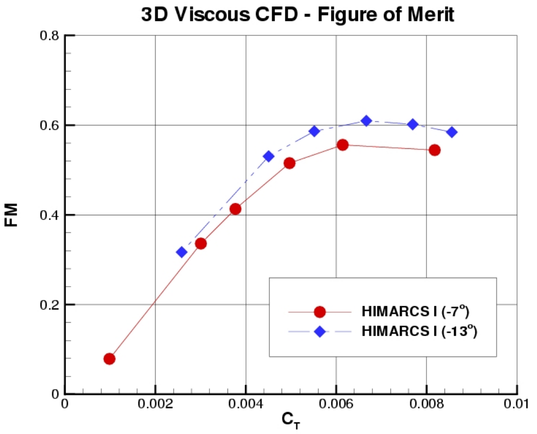

(d)

Figure 10: 3D CFD results showing the effect of blade twist. Inviscid: (a) C_Q vs. C_T. (b) C_T vs. FM. Viscous: (c) C_Q vs. C_T. (d) C_T vs. FM. (M_T = 0.627, Re = 168,602)

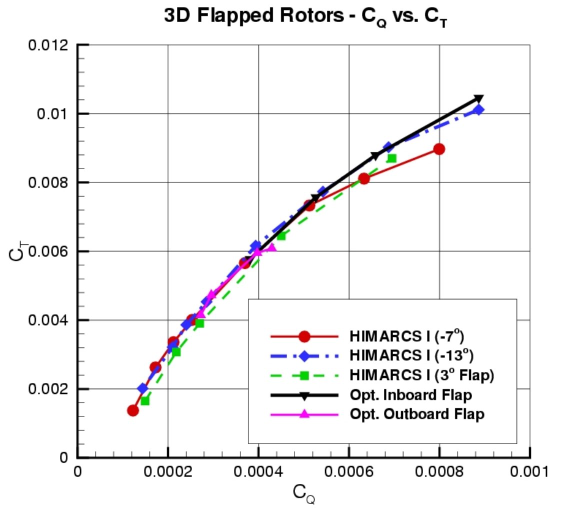

(a)

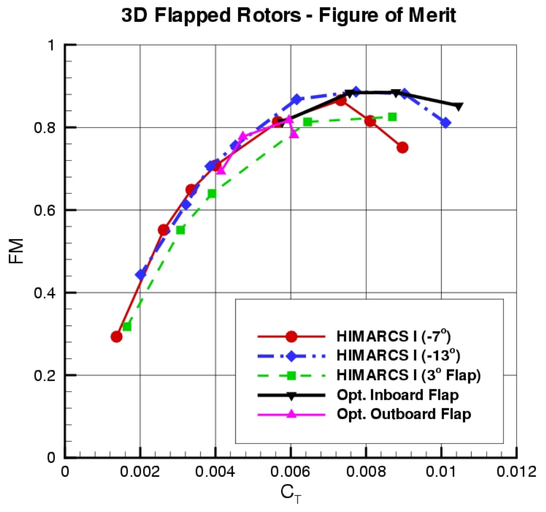

(b)

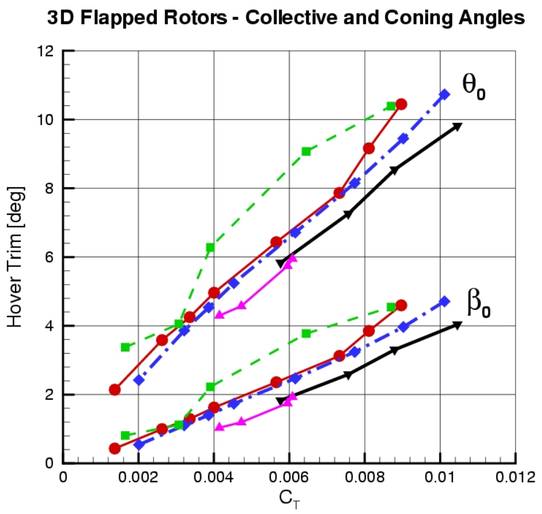

(c)

Figure 11: 3D inviscid CFD results with both inboard and outboard optimised flaps. (a) C_Q vs. C_T. (b) C_T vs. FM. (c) FM vs. Trim. (M_T = 0.627; blade collective taken at 0.75R.)

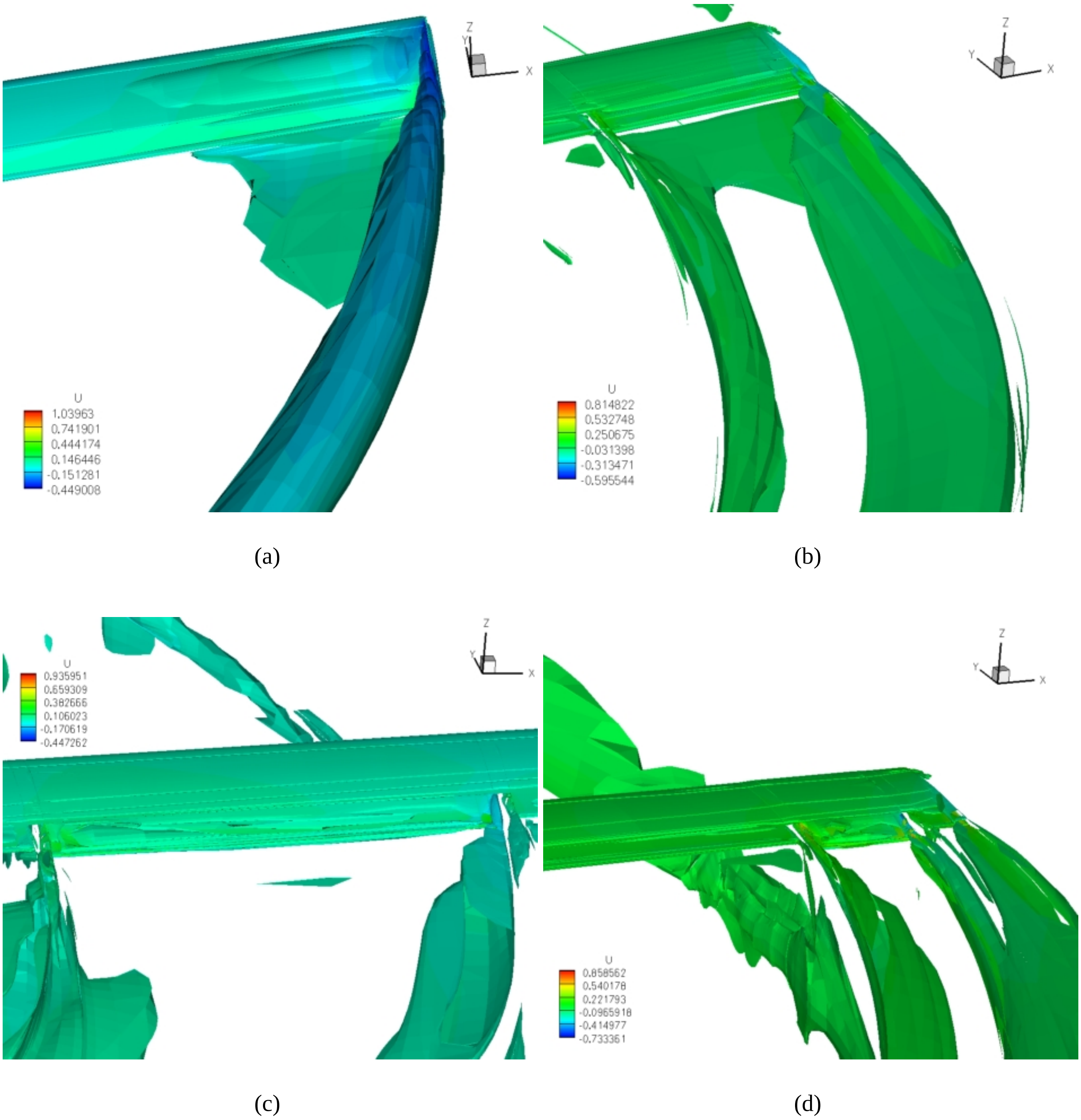

Figure 12: Near wake using iso-surfaces of λ_2 coloured by U velocity. (a) Clean Blade. (b) 3^o slotted flap. (c) Optimum inboard flap. (d) Optimum outboard flap. (M_T = 0.627)

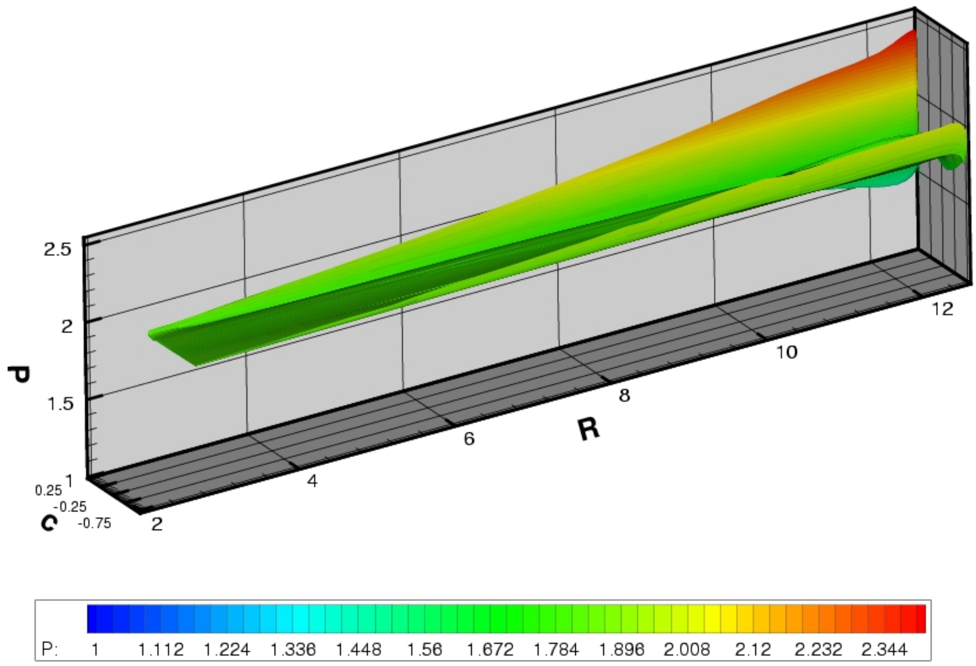

(a)

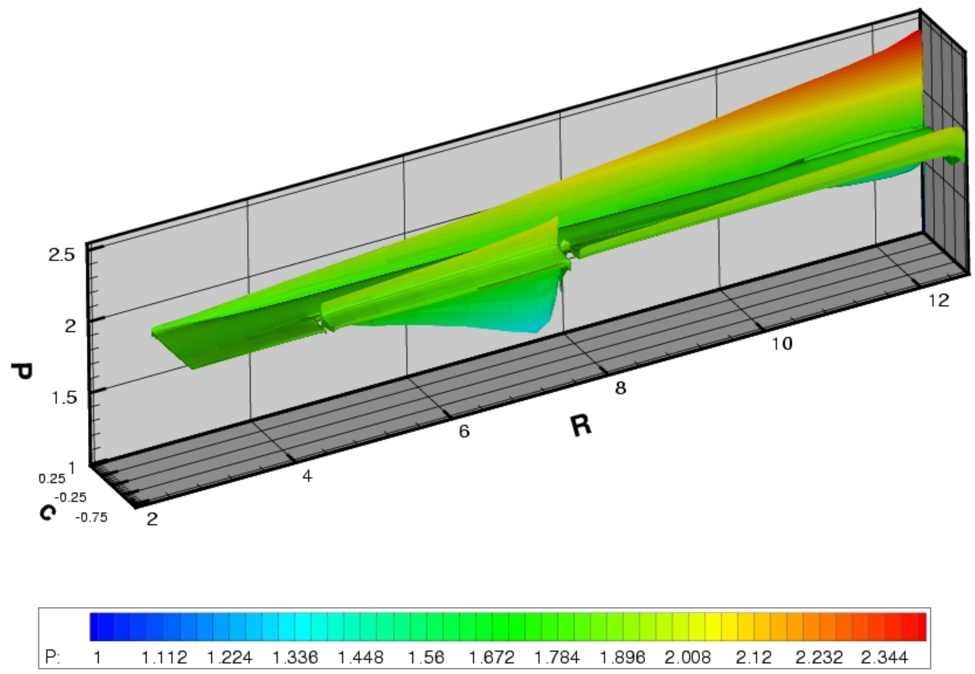

(b)

Figure 13: Pressure distribution along the blade span. (a) Baseline. (b) Inboard flap. (M_T = 0.627, θ_0 = 2.75^o, β_0 = 0^o)

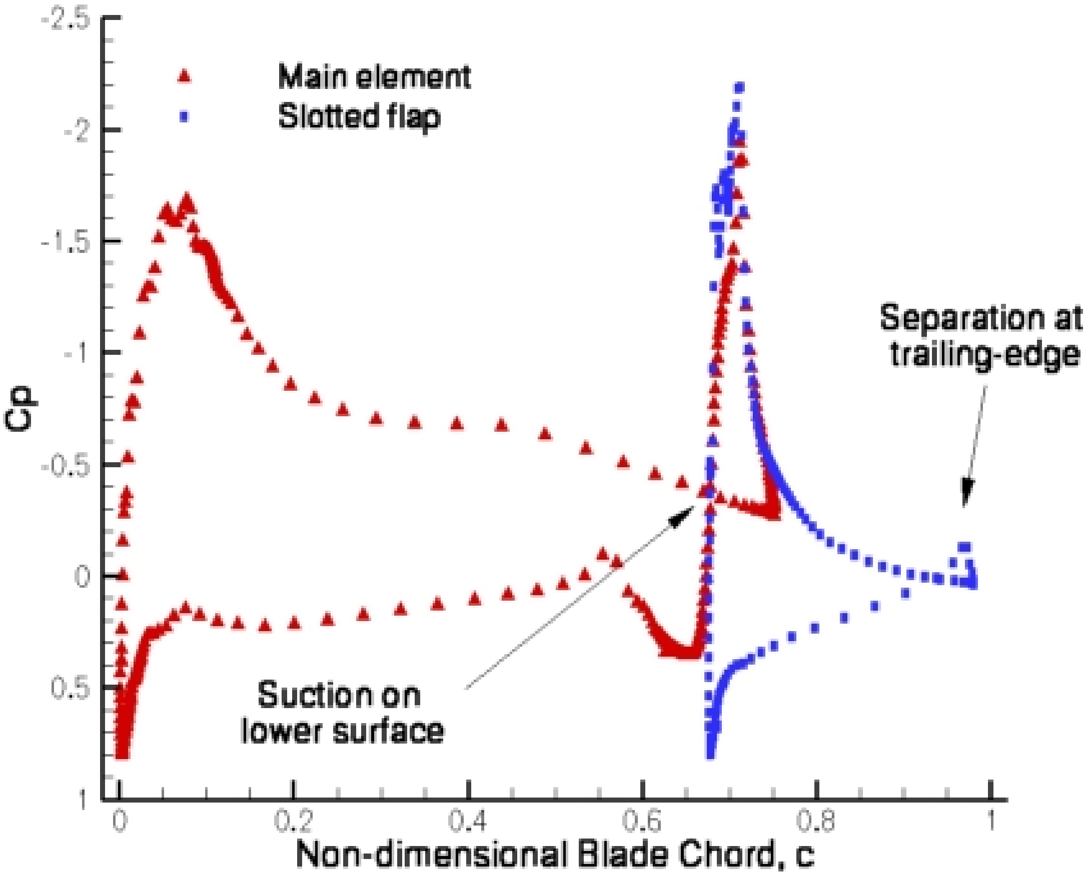

(a)

Figure 14: C_p distribution over the RC(4)-10 section with a slotted flap. (α = 5^o, δ = 10^o, M = 0.5, Re = $5x10^6$)